AD-A179 136 GENERATION OF BROADBAND NOISE IN THE MAGNETOTAIL(U) 1/1
AEROSPACE CORP EL SEGUNDO CA LAB OPERATIONS
P B DUSENBERY ET AL 01 MAR 87 TR-0086(6940-06)-12
UNCLASSIFIED SD-TR-87-12 F04701-85-C-0086 F/G 4/1 NL

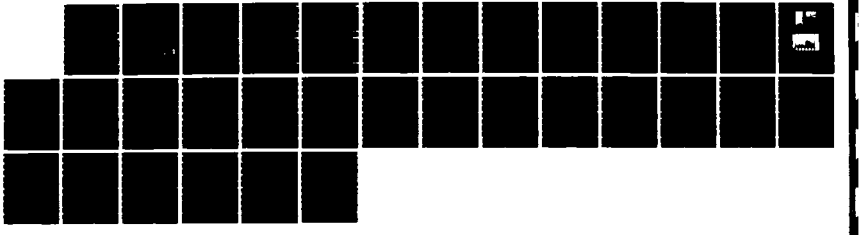

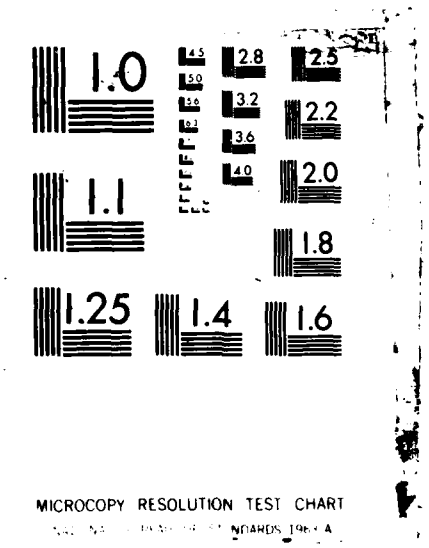

MICROCOPY RESOLUTION TEST CHART

NBS 1963 A

(12)

REPORT SD-TR-87-12

Generation of Broadband Noise in the Magnetotail

P. B. DUSENBERY
Department of Astrophysical, Planetary, and Atmospheric Sciences
University of Colorado
Boulder, CO 80309-0391

and

L. R. LYONS
Space Sciences Laboratory
Laboratory Operations
The Aerospace Corporation
El Segundo, CA 90245

1 March 1987

Prepared for

SPACE DIVISION
AIR FORCE SYSTEMS COMMAND
Los Angeles Air Force Station
P.O. Box 92960, Worldway Postal Center
Los Angeles, CA 90009-2960

This report was submitted by The Aerospace Corporation, El Segundo, CA 90245, under Contract No. F04701-85-C-0086 with the Space Division, P.O. Box 92960, Worldway Postal Center, Los Angeles, CA 90009-2960. It was reviewed and approved for The Aerospace Corporation by H. R. Rugge, Director, Space Sciences Laboratory.

Lt Clarence V. Wilcox/CLTPC was the project officer for the Mission-Oriented Investigation and Experimentation (MOIE) Program.

This report has been reviewed by the Public Affairs Office (PAS) and is releasable to the National Technical Information Service (NTIS). At NTIS, it will be available to the general public, including foreign nationals.

This technical report has been reviewed and is approved for publication. Publication of this report does not constitute Air Force approval of the report's findings or conclusions. It is published only for the exchange and stimulation of ideas.

Clarence V Wilcox

CLARENCE V. WILCOX, Lt, USAF
MOIE Project Officer
SD/CLTPC

Joseph Hess

JOSEPH HESS, GM-15
Director, AFSTC West Coast Office
AFSTC/WCO OL-AB

UNCLASSIFIED

SECURITY CLASSIFICATION OF THIS PAGE

REPORT DOCUMENTATION PAGE

1a. REPORT SECURITY CLASSIFICATION Unclassified	1b. RESTRICTIVE MARKINGS
2a. SECURITY CLASSIFICATION AUTHORITY	3. DISTRIBUTION/AVAILABILITY OF REPORT Approved for public release; distribution unlimited.
2b. DECLASSIFICATION/DOWNGRADING SCHEDULE	
4. PERFORMING ORGANIZATION REPORT NUMBER(S) TR-0086(6940-06)-12	5. MONITORING ORGANIZATION REPORT NUMBER(S) SD-TR-87-12
6a. NAME OF PERFORMING ORGANIZATION The Aerospace Corporation Laboratory Operations 6b. OFFICE SYMBOL (If applicable)	7a. NAME OF MONITORING ORGANIZATION Space Division
6c. ADDRESS (City, State and ZIP Code) El Segundo, CA 90245	7b. ADDRESS (City, State and ZIP Code) Los Angeles, CA 90009-2960
8a. NAME OF FUNDING/SPONSORING ORGANIZATION Space Division 8b. OFFICE SYMBOL (If applicable)	9. PROCUREMENT INSTRUMENT IDENTIFICATION NUMBER F04701-85-C-0086
8c. ADDRESS (City, State and ZIP Code) Los Angeles, CA 90009-2960	10. SOURCE OF FUNDING NOS. PROGRAM ELEMENT NO. / PROJECT NO. / TASK NO. / WORK UNIT NO.
11. TITLE (Include Security Classification) Generation of Broadband Noise in the Magnetotail	
12. PERSONAL AUTHOR(S) Dusenbery, P. B., University of Colorado; Lyons, Lawrence R.	
13a. TYPE OF REPORT 13b. TIME COVERED FROM _____ TO _____	14. DATE OF REPORT (Yr., Mo., Day) 1 March 1987 15. PAGE COUNT 26
16. SUPPLEMENTARY NOTATION	
17. COSATI CODES FIELD / GROUP / SUB. GR.	18. SUBJECT TERMS (Continue on reverse if necessary and identify by block number) Electrostatic Noise Geomagnetic Tail

19. ABSTRACT (Continue on reverse if necessary and identify by block number)

We have evaluated the generation of electrostatic noise in the geomagnetic tail by ion beams. We assume a stationary plasma-sheet electron distribution and streaming ion distributions. Both warm ion streams, as observed within the plasma sheet boundary layer, and cold ion streams, as expected from upward flowing ionospheric ions, are considered. Warm ion streams by themselves are found to be stable, whereas a cold ion stream by itself is unstable to the beam acoustic model. However, wave growth is increased if both cold and warm streams are simultaneously present. These results suggest that the interaction between the warm and cold ion streams is responsible for the peak in electrostatic wave intensities observed within the plasma sheet boundary layer. For cold and warm ions streaming in the same direction, we find wave growth peaks for wave normal angles $\theta = 0°$ and wave frequencies ~0.1 x the electron plasma frequency. However, for anti-parallel streaming cold and warm ions, wave growth peaks near $\theta \approx 90°$ and wave frequencies are an order of magnitude smaller. Including counter streaming warm ions in addition to a cold ion stream results in wave growth that is a superposition of that for the above two cases.

20 DISTRIBUTION/AVAILABILITY OF ABSTRACT UNCLASSIFIED/UNLIMITED ☒ SAME AS RPT. ☐ DTIC USERS ☐	21. ABSTRACT SECURITY CLASSIFICATION Unclassified
22a. NAME OF RESPONSIBLE INDIVIDUAL	22b TELEPHONE NUMBER (Include Area Code) 22c OFFICE SYMBOL

DD FORM 1473, 83 APR EDITION OF 1 JAN 73 IS OBSOLETE.

UNCLASSIFIED

SECURITY CLASSIFICATION OF THIS PAGE

PREFACE

We would like to thank T.E. Eastman and C.Y. Huang for their many helpful comments and for the use of the ISEE 1 wave and particle data from the University of Iowa.

CONTENTS

PREFACE..... 1

1. INTRODUCTION..... 7

2. THEORY AND RESULTS..... 12

3. CONCLUSIONS..... 24

REFERENCES..... 27

FIGURES

1. A Noon-Midnight Meridian Cross Section of the Earth's Magnetosphere Illustrating the Regions of Importance to the Generation of Broadband Electrostatic Noise..... 9

2a. ISEE 1 LEPEDEA Particle Data for Day 85 of 1978..... 10

2b. ISEE 1 SFR Wave Data for Day 895 of 1978..... 10

3. Growth rate, γ, vs. Wave Normal Angle (a) and vs. Normalized Wave Number (b) for a Single Ion Stream. 15

4. A Schematic Illustrating the Difference Between Parallel and Anti-Parallel Streaming of Cold and Hot Ion Distributions in Generating the Beam Acoustic Mode for Different θ's..... 17

5. Frequency (a) and Wave Growth (b) Dependence on Wave Normal Angle, θ, for the Parallel Streaming Case Described in Fig. 4..... 19

6. Dispersion Plots of Normalized Wave Frequency (a) and Normalized Wave Growth (b) vs. Normalized Wave Number for Various Wave Normal Angles..... 20

7. Similar to Fig. 5 Except That v_c = -900 km s^{-1}..... 21

8. Normalized Wave Frequency (a) and Normalized Growth Rate (b) vs. Normalized Wave Number for Various Wave Normal Angles for the Anti-Parallel Streaming Case Considered in Fig. 7..... 22

9. Growth Rate vs. θ for a Given k and Normalized Growth Rate vs. Normalized Wave Number for Various θ's for a Counter Streaming Ion Model..... 23

1. Introduction

Intense electrostatic waves are frequently observed in the plasma sheet region of the earth's magnetotail in the frequency range 10Hz to several kHz with maximum intensities near 10 - 50Hz. The first report of these waves was by Scarf et al. (1974) using IMP 7 data.

Subsequently, Gurnett et al. (1976) made more detailed measurements from the wave experiments on the IMP 8 satellite. In addition to the broad frequency range, Gurnett et al. (1976) found an average rms electric field amplitude of about 1mV/m and were able to deduce that at times the waves propagated within about ± 20° from perpendicular to the magnetic field. The highest frequency of occurrence of the electrostatic noise was found by Gurnett et al. (1976) in the region near the plasma sheet boundary layer when anisotropic fluxes of ions streaming either earthward or anti-earthward were present.

Earthward and anti-earthward streaming ions of keV energies have been observed within the plasma sheet boundary layer using IMP 8 measurements (Frank et al., 1976; DeCoster and Frank, 1979) and ISEE 1 measurements (Williams, 1981; Lui et al., 1983). These particles likely result from energization in the tail current sheet as proposed by Lyons and Speiser (1982). They are dominantly protons with streaming speeds of 500 - 1,500 km/sec, temperatures of 0.1 - 1keV, and densities < $1cm^{-3}$. Their thermal energy is approximately equal to the beam energy.

Cold ion streams of ionospheric origin have been observed in the lobes as well as the plasma sheet (Sharp et al., 1981). The composition of the cold ions is usually H^+ or O^+. Typical number densities are < 0.1 cm^{-3}, temperatures of 50eV or less, and streaming speeds 10 - 1,000 km/s. Figure 1 is a schematic of the noon-midnight meridian cross section of the earth's magnetosphere emphasizing the suggested importance of both ion beams within the plasma sheet boundary layer.

Figure 2 is from Grabbe and Eastman (1984) illustrating the association between ion beams and broadband waves. Figure 2a is the ISEE 1 LEPEDEA particle data for day 85 of 1978 from 0000 to 0600 UT. The ion beam was measured near 0325 UT coincident with the intensification of the measured electrostatic noise by the SFR wave experiment on ISEE 1 (Figure 2b). Prior to and following 0325 UT, ISEE 1 was in the lobe and central plasma sheet, respectively, where the noise was observed to be much weaker (T. Eastman, private communication, 1985). The smooth ion distribution in Figure 2a - C near the origin in velocity space is not real and represents an artificial one count level in the particle detector. In fact, it is very rare for stationary - 100eV ion distributions to be measured when ISEE 1 is either in the lobes or in the plasma sheet boundary layer (C. Huang, private communication, 1985).

Because of the strong correlation between ion beams and broadband noise (Gurnett et al., 1976), it is reasonable to investigate the role played by ion beam instabilities in explaining the generation of broadband waves in the plasma sheet region. Grabbe and Eastman (1984) modeled the plasma sheet particle populations by streaming keV ions, cold stationary ions (- 100eV), and several hundred-eV stationary electrons. They found that broadband waves were

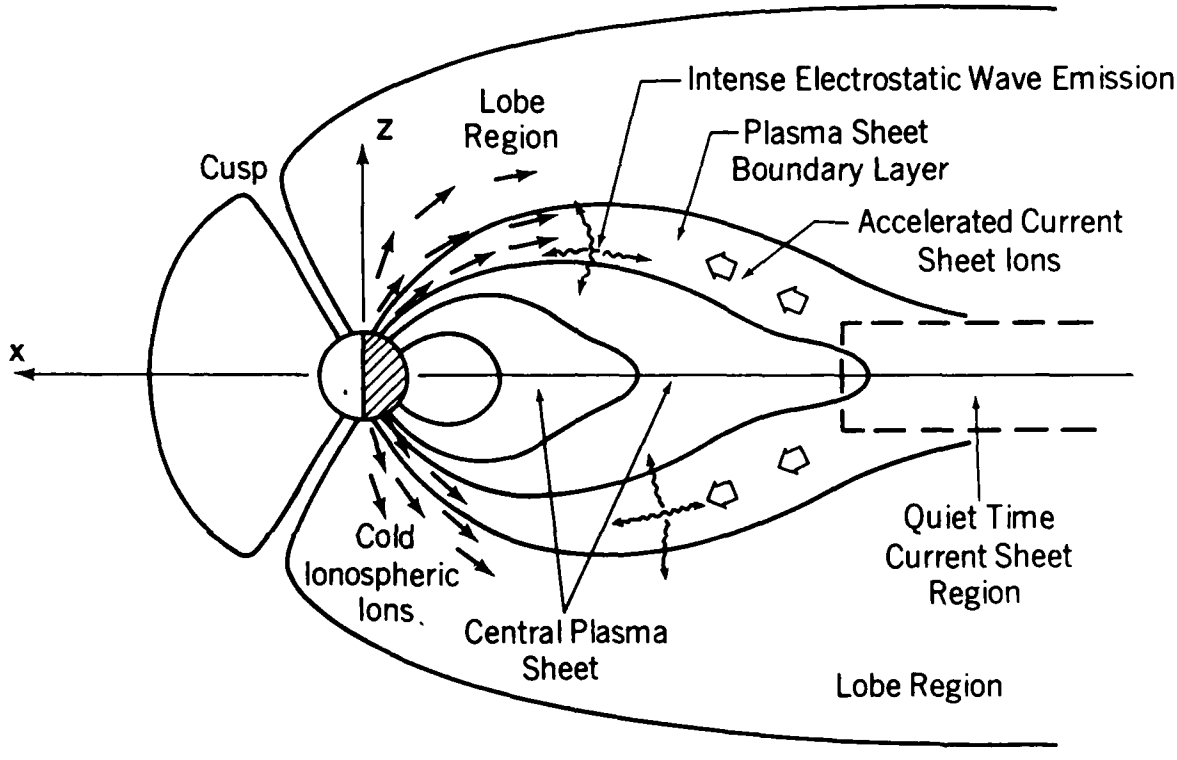

Fig. 1. A Noon-Midnight Meridian Cross Section of the Earth's Magnetosphere Illustrating the Regions of Importance to the Generation of Broadband Electrostatic Noise

(a)

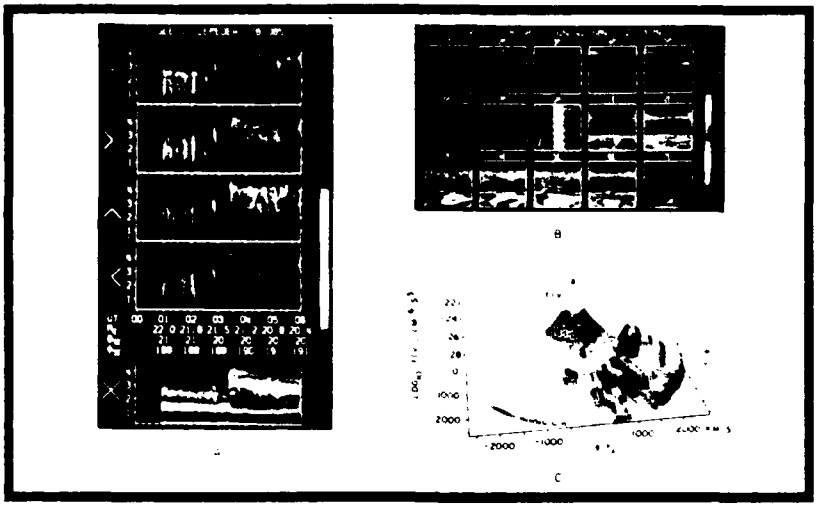

(b)

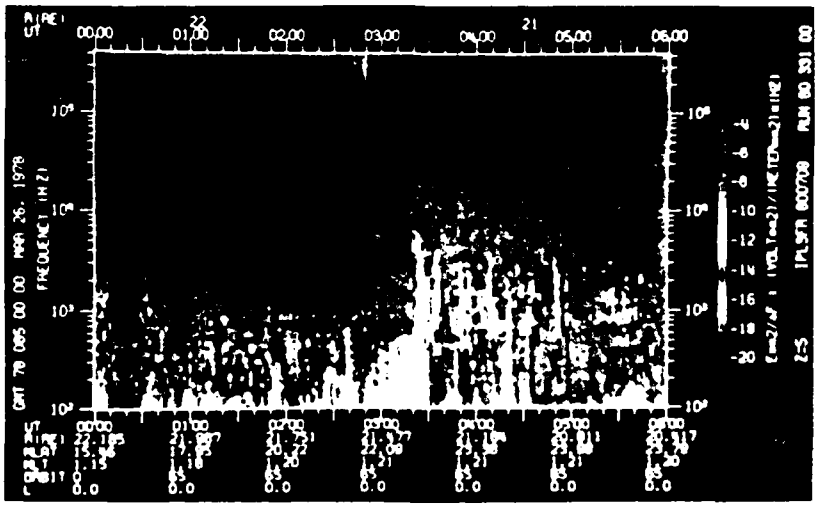

Fig. 2a. ISEE 1 LEPEDEA Particle Data for Day 85 of 1978. (A) Energy vs. time spectrogram from 0000 to 0600 UT. (B) Energy vs. Φ near 0326 UT showing a single beam near $\Phi = 0$. (C) Perspective plot of the three-dimensional ion distribution for 0324:42 to 0326:50 UT when ISEE 1 was in the plasma sheet boundary layer. The smooth distribution centered at the origin of velocity space is artificial.

Fig. 2b. ISEE 1 SFR Wave Data for Day 895 of 1978. Notice that the wave intensity increases near 0324 UT when ISEE 1 enters the boundary layer [courtesy of C. Huang, University of Iowa].

excited only when the ion beams were very cold (thermal energy < 1% of the beam energy). Neither such ion beam thermal energies nor stationary ion distributions are typical of warm plasma sheet boundary layer ions so that the Grabbe and Eastman (1984) study does not explain the association of the intense broadband noise with the warm boundary layer ion beams. In addition, Grabbe and Eastman (1984) calculated that the growth rate of the excited waves decreases with increasing wave normal angle, which cannot explain wave intensities peaking at wave normal angles near 70°. However, Omidi (1985) showed that if the ions are properly treated as unmagnetized, then the distribution model assumed by the Grabbe and Eastman study leads to growth rates that peak near wave normal angles ~ 70°.

Assuming that there are two streaming ion distributions, a warm current sheet population and a cold ionospheric population, Dusenbery and Lyons (1985) investigated the role number density, relative ion drift, and current sheet ion temperature had in destabilizing the fast and slow beam acoustic mode. Their model predicted that the wave intensity of broadband noise should peak in the plasma sheet boundary layer due to the strong interaction between the warm and cold ion beams. Observations of less intense electrostatic waves in the lobes and plasma sheet were likely a result of cold ionospheric beams in the absence of warm ion beams which resulted in smaller growth rates.

A limitation of our previous study was its restriction on wave normal angle (parallel propagating waves were only considered) and its choice of distribution model (ion beams drifting in the same direction). The primary goal of the present study is to investigate several different distributions for the

streaming ions and to evaluate the frequency and growth rate characteristics of the beam acoustic instability as a function of wave number and wave normal angle.

2. Theory and Results

In this report, we assume both ions and electrons are unmagnetized. For the magnetic field in the tail (< 50γ), the wave frequencies we consider are much greater than the ion gyrofrequency ($\lesssim$ 0.8Hz), and the wave numbers k are much greater than ρ_i^{-1} where ρ_i is the ion gyroradius ~ 300km for 300eV H^+ ions.

The complex zeroes of the longitudinal dielectric function, ε (Ichimaru, 1973), give the dispersive properties for waves that are purely electrostatic. From Dusenbery (1986), the solution of ε for unmagnetized ions and electrons is given by

$$\varepsilon(k,\omega') = 1 + \sum_{\alpha} \frac{1}{k^2\lambda_{D\alpha}^2} W(x_\alpha)$$

where

$$x_\alpha = \frac{2^{1/2}}{kV_\alpha} (\omega' - k_\parallel v_\alpha)$$

$$V_\alpha = (2T_\alpha/m_\alpha)^{1/2}$$

$$\lambda_{D\alpha} = (T_\alpha/4\pi\bar{n}_\alpha e^2)^{1/2}$$

$$\omega' = \omega + i\gamma$$

and W is the W function defined by Ichimaru (1973), which is closely related to the plasma dispersion function of Fried and Conte (1961). Parallel ($\parallel$) and perpendicular ($\perp$) refer to directions with respect to a constant, external, plasma sheet magnetic field B_o aligned along the x axis. The subscript α denotes species. The parameter v_α is the streaming speed along B_o, V_α is the thermal speed, $\lambda_{D\alpha}$ is the Debye length, and $\bar{n}_\alpha$ is the number density.

An analytic expression for the beam acoustic wave frequency was derived by Dusenbery (1986) valid for any wave normal angle, θ, given by

$$\omega = k\left[v_c \cos\theta \pm C_s \sqrt{\frac{\bar{n}_c / \bar{n}_e + 3T_c / T_e}{1 + k^2 \lambda_{De}^2}}\right] \qquad (2)$$

where the subscript c refers to the cold ion beams, $C_s = (T_e / m_c)^{1/2}$ is the ion acoustic speed, and $\pm$ refers to the two branches of the beam acoustic mode. Dusenbery and Lyons (1985) showed that the two branches of the beam acoustic mode could be characterized by positive or negative wave energy (W_E) when looked at in the electron rest frame and found that for a single cold ion stream only the slow mode ($W_E < 0$) was growing. Dusenbery (1986) derived an analytic expression for the beam acoustic growth rate (γ) valid for $T_c << T_e$ and $k\lambda_{De} < 1$. Assuming a single cold ion stream ($\bar{n}_e = \bar{n}_c$), then γ for the slow mode is given by

$$\gamma = \frac{\sqrt{\pi}}{2^{3/2}} \sqrt{m_e / m_c}\,[1 + 3T_c / T_e]^{3/2} * \\ * \left(k(v_c \cos\theta - C_s\sqrt{1 + 3T_c / T_e}\right) \qquad (3)$$

As long as $|v_c| > C_s$, equation (3) implies that γ should be maximum at $\theta = 180°$ (for $v_c < 0$ or cold ions streaming anti-earthward) and equal to zero at $\theta = \theta_o$ where

$$\cos \theta_o = C_s \sqrt{1 + 3T_c / T_e} \; / \; v_c \qquad (4)$$

Figure 3 shows γ versus θ in panel (a), and γ/ω_{pe} versus $k\lambda_{De}$ in panel (b) for the slow mode with parameters typical of the plasma sheet region for a single cold ion stream. Using these values, we find from equation (4) that $\theta_o = 111°$ which compares favorably with Figure 3a for the θ at which $\gamma = 0$. Notice from Figure 3b that the growth rate peaks at $k\lambda_{De} \lesssim 1$ with $(\gamma/\omega_{pe})_{max} \approx 4 \times 10^{-4}$. Such growth is due solely to free energy in the resonant electrons. Dusenbery and Lyons (1985) have shown, however, that the beam acoustic growth rate can be significantly enhanced by resonant interactions with a warm streaming current sheet ion distribution. This is the topic we consider next.

While single cold ion streams predominate in the lobe region (Sharp et al., 1981), particle observations in the plasma sheet boundary layer (Williams, 1981; Eastman et al., 1984) indicate that one of the following three conditions usually prevail:

1. Parallel Streaming - warm and cold ion beams drifting in the same direction.
2. Anti-Parallel Streaming - warm and cold ion beams drifting in opposite directions.
3. Counter Streaming - warm and cold ion beams drifting opposite to a warm ion beam.

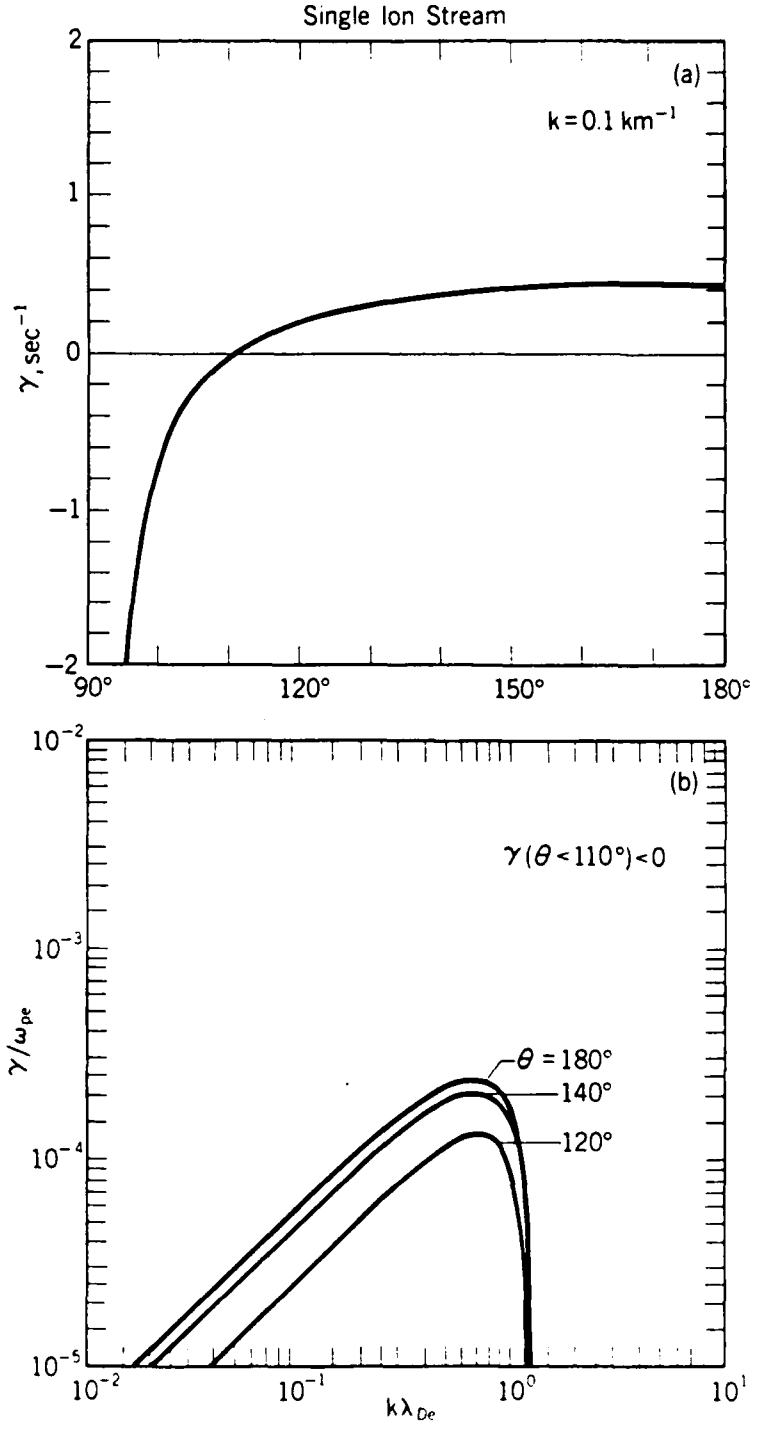

Fig. 3. Growth rate, γ, vs. Wave Normal Angle (a) and vs. Normalized Wave Number (b) for a Single Ion Stream. T_e = 300 eV, T_i = 10 eV, $\bar{n}_e = \bar{n}_i$ = 1 cm^{-3}, and v_i = -500 km s^{-1}.

It is our intent in this report to determine if any model dependence exists in the behavior of the calculated wave frequency and growth rate of the beam acoustic mode for the models considered above.

Omidi (1985) noted that in order to calculate obliquely propagating beam acoustic modes under plasma sheet conditions when the ions were assumed to be unmagnetized, the ion distributions had to be projected onto the phase velocity vector, parallel to the wave vector $\underline{k}$. This projection implies that hot ions with speed $v = \omega/k$ are in Landau resonance with beam acoustic waves which satisfy equation (2). If there are significant numbers of such ions and if they have sufficient free energy, then a strong ion-ion resonant interaction occurs. Figure 4 illustrates the difference between parallel and anti-parallel streaming models for generating the slow beam acoustic mode for different θ's. The x identifies where Landau resonance occurs in velocity space for the θ's considered.

Recall from Dusenbery and Lyons (1985) that the slow mode grows (damped) when resonant particles diffuse to higher (lower) energies in velocity space and such growth (damping) depends upon the velocity gradient in the distribution function at resonance. Thus, Figure 4a predicts that the growth rate for the parallel streaming model should peak at $\theta = 0°$ and decrease with increasing θ. On the other hand, Figure 4b predicts the opposite behavior for the growth rate where a strong ion-ion interaction now occurs for a θ much closer to 90° because the projected distributions are now much closer together in velocity space.

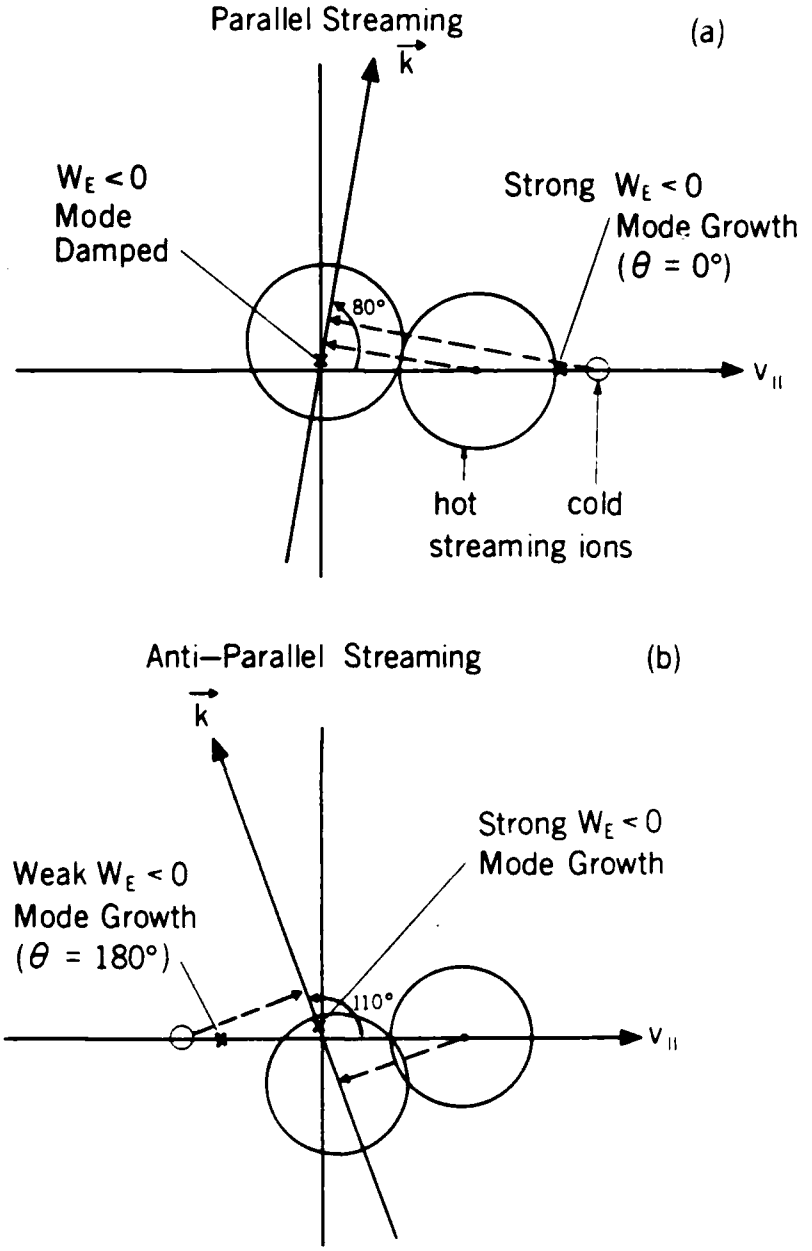

Fig. 4. A Schematic Illustrating the Difference Between Parallel and Anti-Parallel Streaming of Cold and Hot Ion Distributions in Generating the Beam Acoustic Mode for Different θ's. An obliquely propagating beam acoustic wave is in resonance with streaming ions which have an effective drift speed given by projecting the drift velocity onto the wave vector, $\vec{k}$. Wave growth should therefore maximize at $\theta = 0°$ in (a) and $\theta = 110°$ in (b).

Figures 5 and 6 are plots of wave frequency and growth rate versus θ and versus wave number, respectively, for the parallel streaming model. Notice in Figure 5 that the growth rate peaks at $\theta = 0°$ as expected from Figure 4a and that the wave frequency is maximum there. From Figure 6, it is seen that the frequency at peak growth ($k\lambda_{De} \lesssim 1$) occurs near 0.1 f_{pe}, where f_{pe} is the electron plasma frequency. The frequency and growth rate behavior for the anti-parallel streaming model is quite different. Figures 7 and 8 are for the same parameters used in the two previous figures except the drift velocity of the cold ion beam has been reversed. From Figure 7b, the growth rate is quite small for waves propagating along the magnetic field and peaks at a θ close to 90° as expected from Figure 4b. Notice, however, that the wave frequency is small near where the growth rate is maximum. In fact, the frequency at peak growth (see Figure 8) is now $\sim$ 0.01 f_{pe}, nearly a magnitude smaller than the corresponding frequency for the parallel streaming model. The frequency at peak growth for the anti-parallel streaming model can be reduced further by reducing the drift velocity of the cold ions. Comparing Figures 6 and 8 to Figure 3, it is seen that the addition of a warm ion distribution significantly enhances the growth of the beam acoustic instability. The final model we will consider is the counter streaming model.

Including counter streaming warm ion distributions in addition to a cold ion stream with $|v_c| > |v_h|$ results in growth rate behavior that is a superposition of the parallel and anti-parallel streaming models. This behavior is shown in Figure 9a, a plot of growth rate versus θ for $k = 0.1$ km^{-1}. The growth rate is maximum at $\theta = 180°$ due to a parallel streaming interaction, but the growth rate does not monotonically decrease as θ approaches 90°. Instead, an increase in γ is evident near $\theta \approx 100° - 110°$ due to an anti-parallel

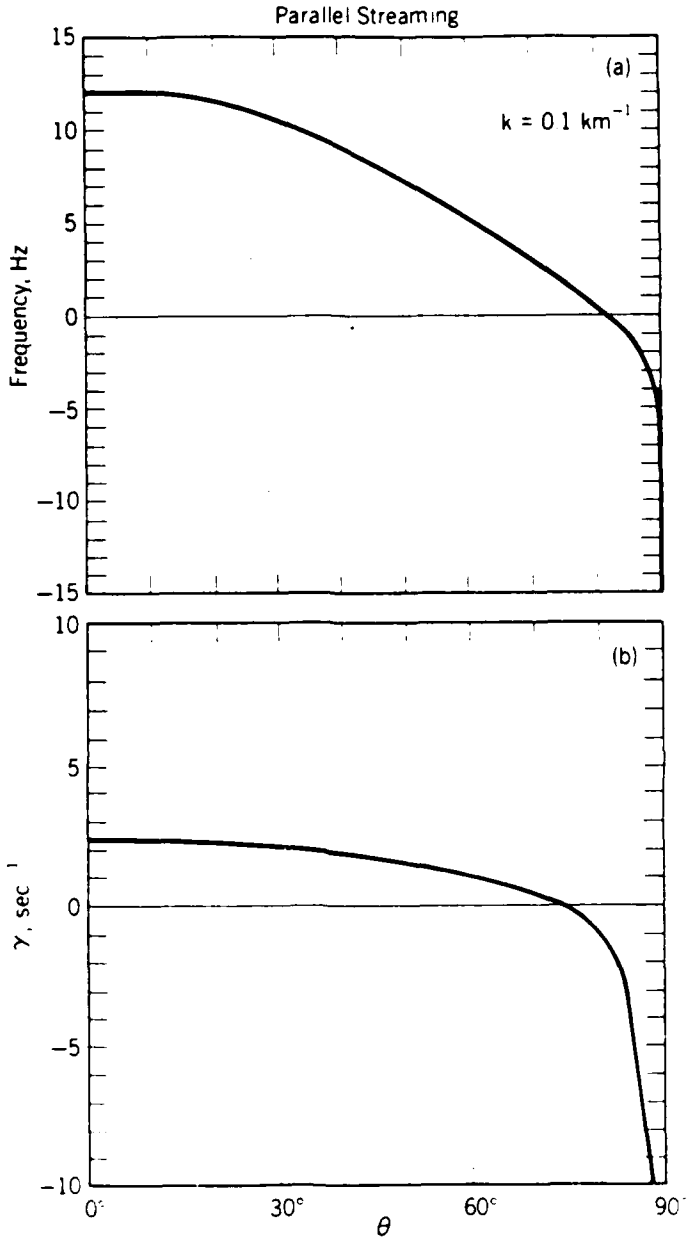

Fig. 5. Frequency (a) and Wave Growth (b) Dependence on Wave Normal Angle, θ, for the Parallel Streaming Case Described in Fig. 4. Wave growth maximizes at $\theta = 0°$. Plasma parameters are $T_e = T_h = 300$ eV, $T_c = 10$ eV; $\bar{n}_c = \bar{n}_h = \bar{n}_e/2$ and $\bar{n}_e = 1$ cm^{-3}; $v_c = 900$ km s^{-1}, and $v_h = 500$ km s^{-1}. The subscript h refers to the warm or hot plasma sheet ion distributions.

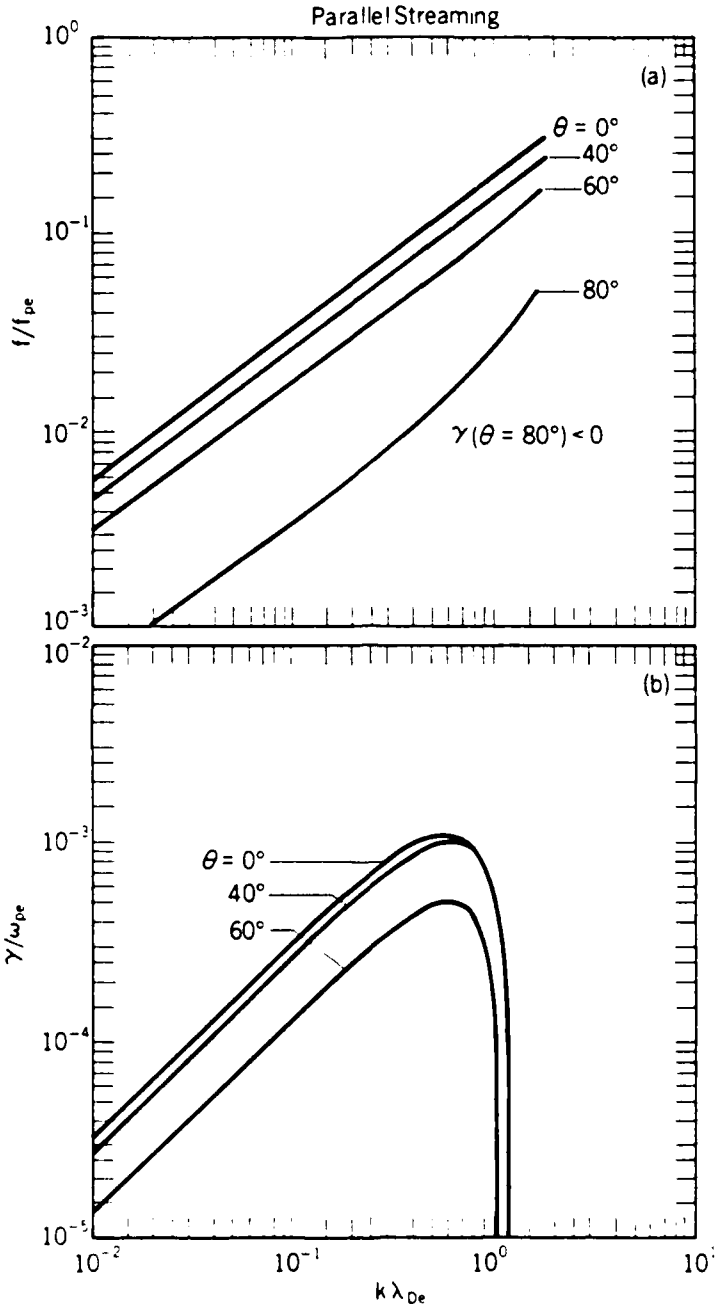

Fig. 6. Dispersion Plots of Normalized Wave Frequency (a) and Normalized Wave Growth (b) vs. Normalized Wave Number for Various Wave Normal Angles. The plasma parameters are defined in Fig. 5.

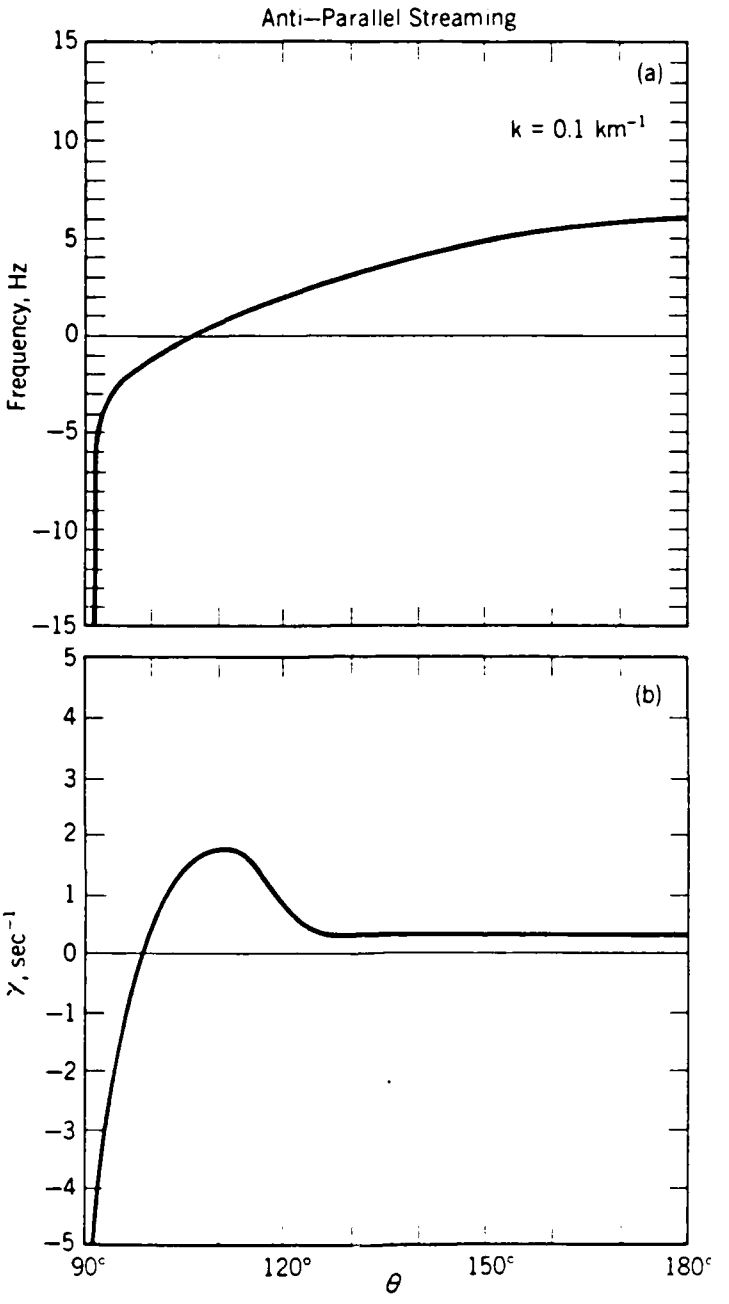

Fig. 7. Similar to Fig. 5 Except That v_c = -900 km s^{-1}. This is an example of the anti-parallel streaming case described in Fig. 4. Wave growth maximizes at $\theta \approx 100°$.

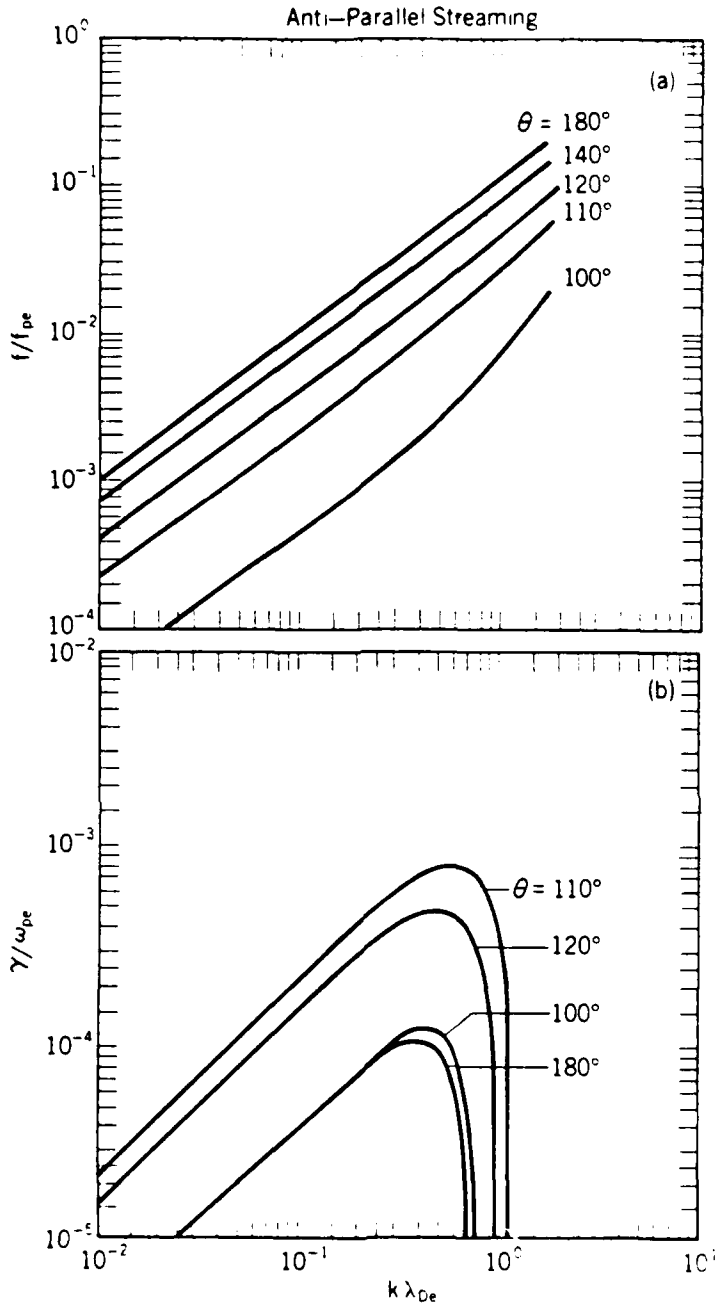

Fig. 8. Normalized Wave Frequency (a) and Normalized Growth Rate (b) vs. Normalized Wave Number for Various Wave Normal Angles for the Anti-Parallel Streaming Case Considered in Fig. 7. Notice that wave growth increases to a maximum value at $\theta \approx 110°$ and then decreases as expected from Fig. 7b.

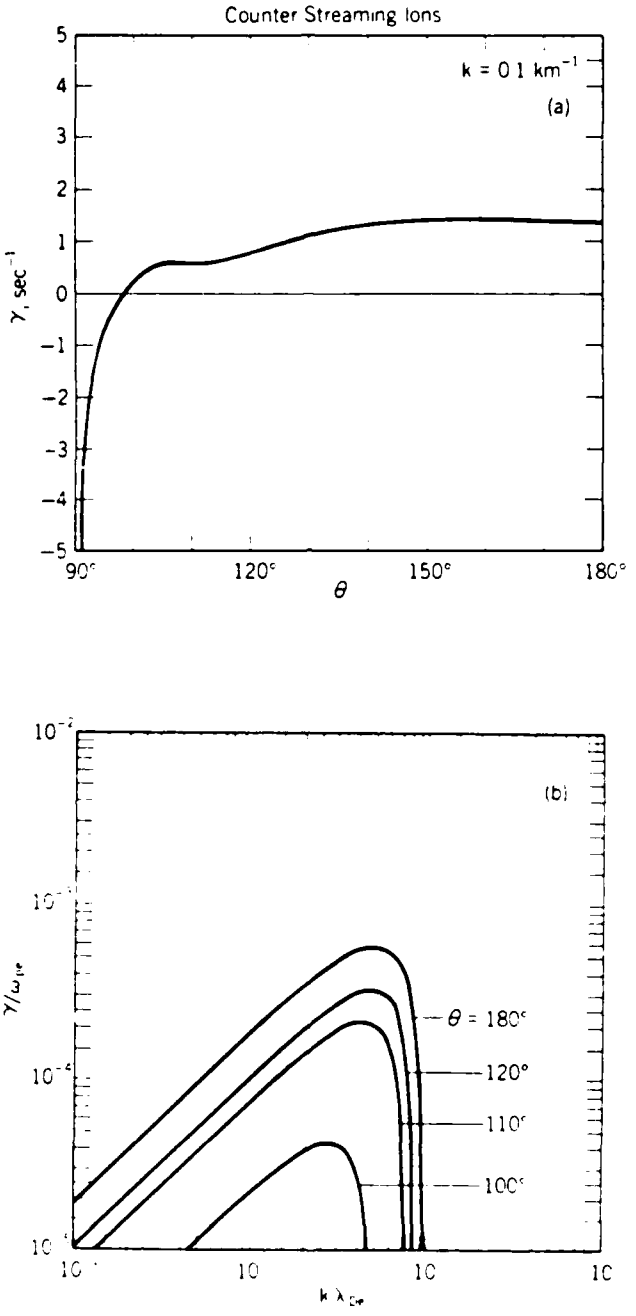

Fig. 9. Growth Rate vs. θ for a Given k and Normalized Growth Rate vs. Normalized Wave Number for Various θ's for a Counter Streaming Ion Model. Plasma parameters are similar to those in Fig. 5 except that v_c = -900 km s^{-1} and v_h = ± 500 km s^{-1}; n_c = 0.4 cm^{-3}, and each hot ion distribution has n_h = 0.3 cm^{-3}.

streaming interaction. The reason the growth rate peak at $\theta \sim 100°$ is not as large as in Figure 7b is due to damping from the $v_h < 0$ ion distribution. In addition, the growth rate of the beam acoustic mode decreases with decreasing number density (Dusenbery and Lyons, 1985). This accounts for the reduction in the overall growth rate for the counter streaming model relative to the two previous models, because the same total ion density ($1 cm^{-3}$) must now be apportioned over three distributions instead of two.

More details concerning the ion beam acoustic mode may be found in Dusenbery (1986) where analytic expressions for the wave frequency and growth rate are derived; i.e., group velocities and amplification lengths for the beam acoustic modes are calculated.

3. Conclusions

We have investigated the generation of electrostatic noise in the plasma sheet region of the geomagnetic tail. The wave intensity of the noise is observed to peak in the plasma sheet boundary layer, but weaker wave events are frequently observed in the tail lobes and central plasma sheet. Previous studies found that if only warm boundary layer ion beams are present, then no broadband waves were excited. However, if cold ion beams (of ionospheric origin) are present, then a growing beam acoustic mode referred to as the slow mode can be excited. If both warm and cold ion beams are present, then both the slow and fast beam acoustic modes may be unstable with growth rates significantly greater than those for a single cold ion beam.

This study focused on the wave frequency and growth rate characteristics of the beam acoustic mode for various particle distribution models. The models were:

1. A single cold ion beam
2. Parallel streaming cold and warm ion beams
3. Anti-parallel streaming cold and warm ion beams
4. Counter streaming warm ion beams and a cold ion beam

Details for each model may be found in Section 2. Single and counter-streaming warm ion beams are stable to the beam acoustic mode in the absence of a cold ion beam. In the rest frame of the plasma sheet electrons, only streaming ions--no stationary ions at the origin in velocity space--were assumed to be present. To date, ISEE 1 particle observations show this assumption to be reasonable for the plasma sheet boundary layer. The single cold ion stream model adequately accounts for the weak wave emissions observed in the lobe. It is argued here and in Dusenbery and Lyons (1985) that the peak wave intensities observed in the plasma sheet boundary layer are a result of cold-warm ion beam interactions.

It has been argued elsewhere in the literature (e.g., Grabbe, 1985; Omidi, 1985) that the peak growth rate of the beam acoustic mode must occur near a wave normal angle close to 90°. Our study finds that this is not always the case, depending upon the combination of ion beams present. In particular, it was found that the growth rate did indeed peak near 90° for the anti-parallel streaming model, but that the growth rate peaked at 0° for the parallel streaming model. In addition to the differences in the behavior of the growth rate for these models, the wave frequency also behaves

differently. The wave frequency at peak growth rate was much larger for the parallel streaming model than for the anti-parallel model. Thus, instances when earthward (warm) and anti-earthward (cold) ion distributions are present imply that the wave intensity should be observed to peak at low frequencies (10-50Hz) with wave normal angles close to 90°. On the other hand, whenever cold and warm parallel streaming ion distributions are present, the wave intensity is predicted to shift to higher frequencies (100-500Hz) and peak for wave normal angles close to 0° (parallel propagating). Including counter streaming warm ions in addition to a cold ion stream results in wave growth that is a superposition of that for the above two models.

In summary, we feel that ion beam instabilities offer a reasonable explanation for the generation of broadband electrostatic noise and adequately account for the observations of such noise not only in the plasma sheet boundary layer, but in the lobes and central plasma sheet regions as well. It must be emphasized that the distribution of wave energy in k-space may not always be predictable from a linear growth rate analysis. Knowing the quasi-linear and non-linear evolution of the instability can only give what the final distribution will be. In this study, we implicitly assume that linear theory is adequate but recognize the need to investigate such non-linear characteristics of the instability as particle diffusion and wave saturation. The wave frequency and growth rate behavior of the noise were found to be sensitive to the choice of particle distribution functions. Thus, the observed noise spectrum and simultaneous particle observations should provide a definitive test for the theory.

REFERENCES

DeCoster, R.J. and L.A. Frank, Observations pertaining to the dynamics of the plasma sheet, J. Geophys. Res., 84, 5099, 1979.

Dusenbery, P.B., L.R. Lyons, The generation of electrostatic noise in the plasma sheet boundary layer, J. Geophys. Res., 90, 10,935, 1985.

Dusenbery, P.B., Generation of broadband noise in the magnetotail by the beam acoustic instability, preprint, 1986.

Eastman, T.E., L.A. Frank, W.K. Peterson, and W. Lennartsson, The plasma sheet boundary layer, J. Geophys. Res., 89, 1553, 1984.

Frank, L.A., K.L. Ackerson, and R.P. Lepping, On hot tenuous plasma, fireballs, and boundary layers in the Earth's magnetotail, J. Geophys. Res., 81, 5859, 1976.

Fried, B.D. and S.D. Conte, The Plasma Dispersion Function, Academic, Orlando, Fla., 1961.

Grabbe, C.L., New results in the generation of broadband electrostatic waves in the magnetotail, Geophys. Res. Lett., 12, 483, 1985.

Grabbe, C.L and T.E. Eastman, Generation of broadband electrostatic noise by ion beam instabilities in the magnetotail, J. Geophys. Res., 89, 3865, 1984.

Gurnett, D.A., L.A. Frank;, and R.P. Lepping, Plasma waves in the distant magnetotail, J. Geophys. Res., 81, 6059, 1976.

Ichimaru, S., Basic Principles of Plasma Physics, W.A. Benjamin, Reading, Mass., 1973.

Lui, A.T.Y., D.J. Williams, T.E. Eastman, and L.A. Frank, Observations of ion streaming during substorms, J. Geophys. Res., 88, 7753, 1983.

Lyons, L.R. and T.W. Speiser, Evidence for Current-Sheet Acceleration in the Geomagnetic Tail, J. Geophys. Res., 87, 2276, 1982.

Omidi, N., Broadband electrostatic noise produced by ion beams in the earth's magnetotail, J. Geophys. Res., 90, 12,330, 1985.

Scarf, F., L. Frank, K. Ackerson, and R. Lepping, Plasma wave turbulence at distant crossings of the plasma sheet boundaries and neutral sheet, Geophys. Res. Lett., 1, 189, 1974.

Sharp, R.D., D.L. Carr, W.K. Peterson, and E.G. Shelley, Ion streams in the magnetotail, J. Geophys. Res., 86, 4639, 1981.

Williams, D.J., Energetic ion beams at the edge of the plasma sheet: ISEE 1 observations plus a simple explanatory model, J. Geophys. Res., 86, 5507, 1981.

LABORATORY OPERATIONS

The Aerospace Corporation functions as an "architect-engineer" for national security projects, specializing in advanced military space systems. Providing research support, the corporation's Laboratory Operations conducts experimental and theoretical investigations that focus on the application of scientific and technical advances to such systems. Vital to the success of these investigations is the technical staff's wide-ranging expertise and its ability to stay current with new developments. This expertise is enhanced by a research program aimed at dealing with the many problems associated with rapidly evolving space systems. Contributing their capabilities to the research effort are these individual laboratories:

Aerophysics Laboratory: Launch vehicle and reentry fluid mechanics, heat transfer and flight dynamics; chemical and electric propulsion, propellant chemistry, chemical dynamics, environmental chemistry, trace detection; spacecraft structural mechanics, contamination, thermal and structural control; high temperature thermomechanics, gas kinetics and radiation; cw and pulsed chemical and excimer laser development including chemical kinetics, spectroscopy, optical resonators, beam control, atmospheric propagation, laser effects and countermeasures.

Chemistry and Physics Laboratory: Atmospheric chemical reactions, atmospheric optics, light scattering, state-specific chemical reactions and radiative signatures of missile plumes, sensor out-of-field-of-view rejection, applied laser spectroscopy, laser chemistry, laser optoelectronics, solar cell physics, battery electrochemistry, space vacuum and radiation effects on materials, lubrication and surface phenomena, thermionic emission, photosensitive materials and detectors, atomic frequency standards, and environmental chemistry.

Computer Science Laboratory: Program verification, program translation, performance-sensitive system design, distributed architectures for spaceborne computers, fault-tolerant computer systems, artificial intelligence, microelectronics applications, communication protocols, and computer security.

Electronics Research Laboratory: Microelectronics, solid-state device physics, compound semiconductors, radiation hardening; electro-optics, quantum electronics, solid-state lasers, optical propagation and communications; microwave semiconductor devices, microwave/millimeter wave measurements, diagnostics and radiometry, microwave/millimeter wave thermionic devices; atomic time and frequency standards; antennas, rf systems, electromagnetic propagation phenomena, space communication systems.

Materials Sciences Laboratory: Development of new materials: metals, alloys, ceramics, polymers and their composites, and new forms of carbon; nondestructive evaluation, component failure analysis and reliability; fracture mechanics and stress corrosion; analysis and evaluation of materials at cryogenic and elevated temperatures as well as in space and enemy-induced environments.

Space Sciences Laboratory: Magnetospheric, auroral and cosmic ray physics, wave-particle interactions, magnetospheric plasma waves; atmospheric and ionospheric physics, density and composition of the upper atmosphere, remote sensing using atmospheric radiation; solar physics, infrared astronomy, infrared signature analysis; effects of solar activity, magnetic storms and nuclear explosions on the earth's atmosphere, ionosphere and magnetosphere; effects of electromagnetic and particulate radiations on space systems; space instrumentation.

...